Hindawi
International Journal of Aerospace Engineering
Volume 2020, Article ID 3085495, 15 pages
https://doi.org/10.1155/2020/3085495

Research Article

Adaptive Fixed-Time Terminal Sliding Mode Control on SE(3) for Coupled Spacecraft Tracking Maneuver

Kejie Gong, Ying Liao, and Yong Wang

College of Aerospace Science and Engineering, National University of Defense Technology, No. 109 Deya Road, Changsha, Hunan 410073, China

Correspondence should be addressed to Kejie Gong; gkjnuaa@163.com

Received 19 November 2019; Revised 17 December 2019; Accepted 2 January 2020; Published 4 February 2020

Academic Editor: James D. Biggs

In this paper, a reaching law-based adaptive fixed-time terminal sliding mode control law, which is used for coupled spacecraft tracking maneuver in the presence of large inertia parametric uncertainties and external disturbances, is proposed. The coupled 6-DOF kinematics and dynamics for spacecraft motion are modeled on Lie group SE(3). The relative configuration is expressed by a local coordinate (exponential coordinate) of SE(3). In order to estimate the inertia parameters and external disturbances, we also propose a novel adaptive update law, which can make the control law be applied without the inertia parameters of the spacecraft a priori. Fixed-time convergence property of the closed-loop feedback system is proved in the framework of Lyapunov. Numerical simulations are performed to demonstrate the performances of the proposed control scheme for coupled spacecraft tracking maneuver.

1. Introduction

Spacecraft proximity operation plays an important role in a variety of space missions such as space debris removal, space station maintenance and installation, on-orbit spacecraft service, large structure assembly, and spacecraft networking [1, 2], in which position and attitude tracking maneuvers are the key steps requiring to be performed with high control precision. So far, the rotational and translational maneuvers of spacecraft were easy to implement separately by ignoring their coupling, but difficult to provide fast and accurate control to meet the requirements of future space missions [3]. Different from the separated control strategy, spacecraft proximity operation needs a precise integral control strategy of coupled 6-DOF motion for the chaser spacecraft [4]. Modeling of coupled rotational and translational relative motions of rigid spacecraft has been receiving great interests in recent years based on different forms, such as dual quaternion [4–7], three-dimensional (3-D) Euclidean space (Lie group SE(3)) [8–11], 6-DOF Euler-Lagrange form [12] (translational motion described in LVLH (local-vertical-local-horizontal) frame and rotational motion described by MRPs (modified Rodrigues parameters)) or other forms [13–18] (translational motion described in body-fixed frame or LOS (line-of-sight) frame and rotational motion described by MRPs). However, dual quaternion inherits the ambiguities intrinsic of quaternion, which may cause unwinding problem. In addition, MRPs describing attitude in Ref. [12] are nonglobal and nonunique. In this study, the kinematics and dynamics of spacecraft relative motion are modeled in unified forms on Lie group SE(3). Lie group SE(3) is the set of positions and attitudes of a rigid body in a 3-D Euclidean space [19, 20] and can represent the spacecraft's motion in a unique and nonsingularity way [21]. Control problem of the 6-DOF spacecraft maneuver modeled on SE(3) has been studied mainly by Lee et al. [8, 22], Sanyal et al. [23], Zhang et al. [11], Nazari et al. [24], Holguin et al. [25], and Jiang et al. [26]. However, they tackled the 6-DOF control problem with sliding mode or terminal sliding mode in the frame of asymptotic or finite-time convergence. The spacecraft control problems with fixed-time stabilization were studied in Refs. [16–18, 27–30]. The attitude control problem with fixed-time stabilization is studied in Ref. [27–29]. Hu et al. [30] considered the fixed-time convergence of position

control for the spacecraft rendezvous mission. For spacecraft 6-DOF fixed-time control problem, the motion is modeled in a nonunified form (LOS frame to describe translational motion and MRPs to describe rotational motion) [16–18]. Different from the aforementioned researches, this study proposes a fixed-time control for spacecraft 6-DOF motion modeled on SE(3) using terminal sliding mode, which achieves a faster convergence rate than asymptotic or finite-time control. Lie group SE(3) is used for analyzing the relative motion. It provides a global analysis for the system, and thus, it is suitable for the relative motion of the spacecraft with any type of orbits, including parabolic or hyperbolic trajectories [31]. While Huang and Jia [16–18] treated the 6-DOF modeling based on a nonglobal analysis method where the model of relative position motion is approximate. In order to represent the translational and rotational motions in a unified form, exponential coordinates are used for representing the relative pose (including attitude and position) via logarithm from SE(3) to se(3), where se(3) is isomorphism with $\mathbb{R}^6$ [8]. Most researches apply the exponential coordinate of SE(3) at the kinematical level. Jiang et al. [26] first derived the second-order derivative of exponential coordinates at the dynamical level and designed an asymptotic control law for the spacecraft hovering over an asteroid.

A spacecraft moving in the outer space is affected by a variety of disturbance forces and torques, including environmental and nonenvironmental influences. Moreover, the inertia parameters of spacecraft may not be known accurately but must be considered in the design of a control scheme. The existence of inertia parametric uncertainties and external disturbances makes the controller design more complicated [31]. Wu et al. [32] developed an adaptive sliding mode control scheme for 6-DOF synchronized control problem, which guarantees fast convergence rate, accurate control results, and no chattering, in the presence of control input constraints, unknown model system parameters, and external disturbances. Lv et al. [33] treated the 6-DOF synchronized control problem of space craft formation flying (SFF) task in the presence of uncertainties, external disturbances, and control saturation constraint. Hu et al. [34, 35] investigated the spacecraft attitude control problem with actuator saturation in the presence of no information about inertia and external disturbances. BoÏskovic et al. [36] proposed a continuous and globally stable tracking control algorithm for spacecraft attitude control problem in the presence of parametric uncertainties, external disturbances, and control input saturation. Filipe and Tsiotras [6] proposed a nonlinear adaptive controller for satellite position and attitude tracking in proximity operations, and the proposed controller requires no prior information about the inertia parameters of the chaser satellite. The gravity-gradient torque, the perturbing forces caused by Earth's oblateness, and persistent external disturbances (but otherwise unknown) are all taken into account. Huang and Jia [16–18] investigated the fixed-time 6-DOF tracking control problem of a spacecraft fly-around task for a noncooperative target in the presence of parametric uncertainties and external disturbances.

In this study, inspired by the adaptive asymptotic stabilization of position and attitude tracking problem that modeled by dual quaternion in Ref. [6], we extend the asymptotic stable control law with dual quaternion to the adaptive fixed-time terminal sliding mode control law on SE(3). In general, to develop the adaptive update law for inertia parameters, the products of the inertia matrix and other vectors are converted to the products of the regression matrices and inertia vector like in Ref. [12], while the update law for inertia parameters in this study requires no regression matrices, but just a simple operator for vectors related to inertia matrix. A fixed-time-type terminal sliding mode surface using the exponential coordinate of the pose is defined. And a fixed-time-type reaching law is applied to drive the tracking errors to converge to the equilibrium points in fixed time. The proposed adaptive control law and update law can be applied without inertia parameters and upper bounds of external disturbances, which guarantees the relative pose and velocities converging to the origins in fixed time from any given initial state, except that the initial relative error of principal rotation angle is exactly π radian. The proposed control scheme for coupled tracking maneuver guarantees the coupled rotational and translational tracking errors almost global fixed-time convergence over $SE(3) \ltimes \mathbb{R}^6$. Thus, the desired pose and velocities can be obtained in fixed time by performing the proposed maneuvering scheme in the presence of inertia parametric uncertainties and external disturbances.

The contributions of this research are as follows: An adaptive modified fixed-time terminal sliding control law (AMFixed) is proposed for coupled spacecraft tracking maneuver that modeled on SE(3), so that the desired pose and velocities are obtained in fixed time in the presences of large inertia parametric uncertainties and external disturbances. The fixed-time control for spacecraft modeled on SE(3) in this study is firstly proposed, and the adaptive update law for inertial parameters is firstly extended from dual quaternion to SE(3). The modified fixed-time terminal sliding controller achieves a faster convergence rate than finite-time one (AFinite) for spacecraft relative motion in [9–12]. Moreover, the proposed modified controller (AMFixed) in this study can reach higher accuracy than the conventional one (AFixed) even the inertia parameters and disturbances are not accurately identified.

The rest of this paper is as follows: The second section presents the rigid body dynamics of the spacecraft on SE(3). The third section explains the design and proofs of the adaptive fixed-time terminal sliding mode control on SE(3). The fourth section shows the simulation results of the proposed control laws. The last section concludes a summary of this research.

Throughout the paper, some notations need to be predefined. Superscript T and -1 denote the transposition operation and inverse operation of a matrix, respectively. $|\cdot|$ means the absolute value. $\|\cdot\|$ denotes the 2-norm of a vector. Vector $x = [x_1, x_2, \cdots, x_n]^T$ and constant γ define the function $\mathrm{sig}(x)^\gamma = [|x_1|^\gamma \ \mathrm{sgn}\ (x_1), |x_1|^\gamma \ \mathrm{sgn}\ (x_2), \cdots, |x_1|^\gamma \ \mathrm{sgn}\ (x_n)]^T$, where sgn $(\cdot)$ is the signum function.

2. Rigid Body Dynamics of Spacecraft on SE(3)

This section presents the 6-DOF kinematics and dynamics of a spacecraft moving on orbit around the earth and relative 6-DOF dynamics of the spacecraft tracking system. First of all, to describe the relative motion dynamics between two spacecrafts, three orthogonal coordinate systems are defined. The Earth-Centered Inertial (ECI) reference frame is denoted by $\{E\} = \{E_x, E_y, E_z\}$, which is usually used for describing absolute motion of a spacecraft around the earth. The leader and follower spacecrafts are both assumed to be rigid bodies. $\{B^0\} = \{B_x^0, B_y^0, B_z^0\}$ and $\{B\} = \{B_x, B_y, B_z\}$ are used for denoting the body-fixed frames with respect to the two spacecrafts. Spacecraft coupled translational and rotational maneuver for the proximity operation is shown in Figure 1.

2.1. Rigid Motion on Lie Group SE(3) and Kinematics of the s121 Spacecraft. The special Euclidean group (Lie group SE(3)) is the configuration space for a rigid body motion in a 3-D Euclidean space, including rotational and translational motions. Lie group SE(3) is the semiproduct of $\mathbb{R}^3$ and SO(3), which is expressed by $\mathrm{SE}(3) = \mathbb{R}^3 \ltimes \mathrm{SO}(3)$. $\mathbb{R}^3$ is 3-D real Euclidean space denoting the position of the spacecraft, and SO(3) is the special orthogonal group describing the rotation of the spacecraft in a 3-D space. Thus, the configuration of the spacecraft motion is expressed as

$$g = \begin{bmatrix} R & p \\ 0_{1\times 3} & 1 \end{bmatrix}, \tag{1}$$

where R denotes the attitude matrix rotated from the spacecraft body-fixed frame $\{B\}$ to the inertial frame $\{E\}$, p represents the position of the spacecraft expressed in the ECI frame, and $0_{m\times n}$ denotes the all-zero matrix with m rows and n columns.

The angular velocity ω and translational velocity v expressed in the spacecraft's body-fixed frame are defined in a unified form as

$$\xi = \begin{bmatrix} \omega \\ v \end{bmatrix} \in \mathbb{R}^6. \tag{2}$$

To describe the kinematics and dynamics of a spacecraft, the following mapping operations need to be defined. The adjoint operator of $g \in \mathrm{SE}(3)$ is defined as

$$\mathrm{Ad}_g = \begin{bmatrix} R & 0_{3\times 3} \\ [p \times R] & R \end{bmatrix} \in \mathbb{R}^{6\times 6}. \tag{3}$$

The operator $[\cdot]^\times$ is the skew-symmetric transformation of a vector in $\mathbb{R}^3$ or cross-product. The velocity mapping from $\mathbb{R}^6$ to se(3) is

$$\xi^\vee = \begin{bmatrix} \omega^\times & v \\ 0_{1\times 3} & 0 \end{bmatrix} \in \mathrm{se}(3), \tag{4}$$

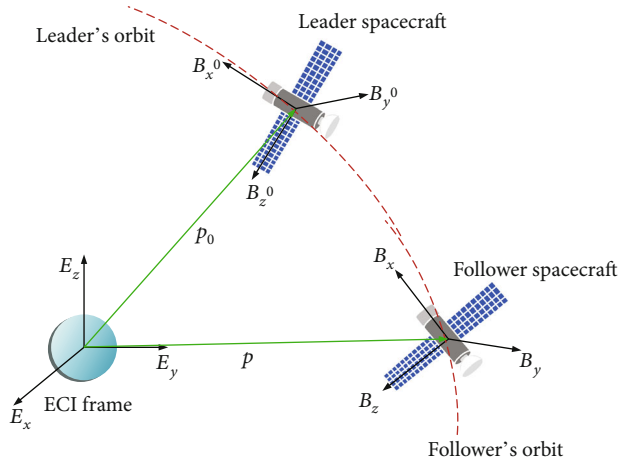

Figure 1: Spacecraft coupled translational and rotational maneuvers.

where se(3) denotes the Lie algebra of Lie group SE(3) which is also called the tangent space at identity. The adjoint operation of se(3) is presented in a block matrix form as

$$\mathrm{ad}_\xi = \begin{bmatrix} \omega^\times & 0_{3\times 3} \\ v^\times & \omega^\times \end{bmatrix} \in \mathbb{R}^{6\times 6}. \tag{5}$$

Here follows the coadjoint operation of se(3) which can be expressed by a 6-by-6 matrix as

$$\mathrm{ad}_\xi^* = \left(\mathrm{ad}_\xi\right)^T = \begin{bmatrix} -\omega^\times & v^\times \\ 0_{3\times 3} & -\omega^\times \end{bmatrix}. \tag{6}$$

In addition, the kinematics of the spacecraft can be expressed as follows:

$$\begin{aligned} \dot{R} &= R[\omega^\times], \\ \dot{p} &= Rv, \end{aligned} \tag{7}$$

where $\dot{R}$ and $\dot{p}$ are the angular velocity and translational velocity expressed in the inertial frame, respectively. Then kinematics (7) can be rewritten in a compact form as

$$\dot{g} = g(\xi)^\vee. \tag{8}$$

2.2. Dynamics of a Spacecraft. The dynamics equations of rotational and translational motions for a rigid spacecraft are presented as

$$\begin{aligned} J\dot{\Omega} &= J[\Omega^\times]\Omega + M_g(p, R) + T_c(p, R, v, \Omega) + T_d, \\ m\dot{v} &= m[v^\times]\Omega + F_g(p, R) + mR^T a_{J_2}(p) F_c(p)(p, R, v, \Omega) + F_d, \end{aligned} \tag{9}$$

where $T_c \in \mathbb{R}^3$ and $F_c \in \mathbb{R}^3$ denote the control torque and control force performed by the spacecraft acting on itself, respectively; $M_g \in \mathbb{R}^3$ and $F_g \in \mathbb{R}^3$ denote the gravity gradient moment and gravity force, respectively; and $T_d \in \mathbb{R}^3$

and $F_d \in \mathbb{R}^3$ denote the unknown torques and forces on the spacecraft, respectively, which are mainly caused by radiation pressure, atmosphere drag, and other bounded uncertain disturbances.

$$M_g = 3\left(\frac{\mu}{\|p\|^5}\right)\left(\left[b^\times\right]Jb\right),$$
$$F_g = -\left(\frac{m\mu}{\|p\|^3}\right)b, \tag{10}$$

where $b = R^T p$ and $\mu = 398,600.44\,\mathrm{km}^3\,\mathrm{s}^{-2}$ is the gravitational constant of the Earth. The perturbation caused by the Earth's oblateness J_2 expressed in ECI frame is given as follows [37]:

$$a_{J_2} = -\frac{3\mu J_2 {R_e}^2}{2\|p\|^5}\begin{bmatrix} p_x\left(1-\frac{5{p_z}^2}{\|p\|^2}\right) \\ p_y\left(1-\frac{5{p_z}^2}{\|p\|^2}\right) \\ p_z\left(3-\frac{5{p_z}^2}{\|p\|^2}\right)\end{bmatrix}, \tag{11}$$

where p_x, p_y, p_z are the components of p, $J_2 = 0.00108263$, and $R_e = 6378\mathrm{km}$ is the equatorial radius of the Earth.

By employing the coadjoint operator of se(3), combining the gravity moment and force on the spacecraft given by (10), and combining the moment of inertia and mass, the rotational and translational dynamics equation (9) can be expressed in a compact form as [8]

$$\mathbb{I}\dot{\xi} = \mathrm{ad}^*_\xi \mathbb{I}\xi + \tau_g + \tau_c + \tau_d. \tag{12}$$

$$\tau_g = \begin{bmatrix} M_g \\ F_g + mR^T a_{J_2}\end{bmatrix},$$
$$\tau_c = \begin{bmatrix} T_c \\ F_c\end{bmatrix},$$
$$\tau_d = \begin{bmatrix} T_d \\ F_d\end{bmatrix}, \tag{13}$$
$$\mathbb{I} = \begin{bmatrix} J & 0_{3\times3} \\ 0_{3\times3} & mI_3\end{bmatrix},$$

where $\tau_g \in \mathbb{R}^6$ is a unified vector which consists of gravity gradient moment and force (including perturbation cause by J_2), $\tau_c \in \mathbb{R}^6$ is a unified vector which consists of control torque and force performed by the spacecraft actuator, and $\tau_d \in \mathbb{R}^6$ is a unified vector which consists of external disturbance torques and forces acting on the spacecraft.

The variables presented at previous are used for describing the kinematics and dynamics of the follower spacecraft. By adding superscript 0, all the kinematics and dynamics variables switch to denote variables of the leader spacecraft. In this study, the leader spacecraft is supposed to move in the gravity field and subject to no control inputs and no external disturbances. Thus, kinematics and dynamics equations of the leader spacecraft in compact forms are

$$\dot{g}^0 = g\left(\xi^0\right)^\vee, \tag{14}$$

$$\mathbb{I}^0\dot{\xi}^0 = \mathrm{ad}^*_{\xi^0}\mathbb{I}^0\xi^0 + \tau^0_g. \tag{15}$$

These two equations can be used for generating trajectories when initial states $(g^0(t_0), \xi^0(t_0))$ at time t_0 are known.

2.3. Relative Coupled Rotational and Translational Dynamics of Spacecraft. This subsection presents the relative coupled rotational and translational dynamics on SE(3). Let $h \in \mathrm{SE}(3)$ represent the actual relative pose between the two spacecrafts and $h_d \in \mathrm{SE}(3)$ represents the desired relative pose. The desired relative pose is assumed to be a fixed configuration, which means that the desired relative velocities are all zeros. Then the configuration tracking error can be described by using h and h_d. The actual relative configuration is given by $h = (g^0)^{-1}g$, and then the pose tracking error is given by

$$h_e = h_d^{-1}h = h_d^{-1}\left(g^0\right)^{-1}g. \tag{16}$$

The exponential coordinate is used for expressing the configuration tracking error of the follower spacecraft, which can be expressed as

$$\tilde{\eta}^\vee = \mathrm{logm}\left((h_d)^{-1}h\right), \tag{17}$$

where logm is the logarithm map from SE(3) to se(3). The vectorized exponential coordinate of the pose tracking error is expressed as

$$\tilde{\eta} = \begin{bmatrix}\tilde{\Theta} \\ \tilde{\beta}\end{bmatrix} \in \mathbb{R}^6, \tag{18}$$

where $\tilde{\Theta} \in \mathbb{R}^3$ and $\tilde{\beta} \in \mathbb{R}^3$ are attitude tracking error and position tracking error, respectively, which are expressed by the exponential coordinate vectors as

$$\tilde{\Theta}^\times = \begin{cases} 0, & \theta = 0, \\ \dfrac{\theta}{2\sin\theta}\left(\tilde{R} - \tilde{R}^T\right), & \theta \in (-\pi \quad \pi), \theta \neq 0. \end{cases}$$
$$\tilde{\beta} = S^{-1}\left(\tilde{\Theta}\right)\tilde{p}, \tag{19}$$

where $\tilde{R}$ is the attitude error matrix and $\tilde{p}$ is the position error vector. $S(\tilde{\Theta})$ is expressed in Ref. [38]. The logarithm map (logm) of matrix from SE(3) to se(3) is bijective when $\|\Theta\| < \pi$.

By taking the time derivative of equation (16) and substituting (14) into (8), the velocity tracking error of the follower spacecraft with respect to the leader spacecraft, which is expressed in the follower's body-fixed frame, is obtained

$$\tilde{\xi} = \xi - \mathrm{Ad}_{h-1}\xi^0, \tag{20}$$

where $\mathrm{Ad}_{h-1}\xi^0$ denotes the leader's unified velocity expressed in the follower spacecraft body-fixed frame.

The kinematics equation expressed by local coordinates is as follows [38]:

$$\dot{\tilde{\eta}} = G(\tilde{\eta})\tilde{\xi}. \tag{21}$$

The computation method for $G(\tilde{\eta})$ is described as follows: From Ref. [38], $G(\eta) \in \mathbb{R}^{6\times 6}$ is expanded as

$$G(\eta) = I_{6\times 6} + \frac{1}{2}\mathrm{ad}_\eta + a(\theta)\mathrm{ad}_\eta^2 + b(\theta)\mathrm{ad}_\eta^2, \tag{22}$$

where

$$\begin{aligned}\theta^2 a(\theta) &= 2 - \frac{3}{4}\theta\cot\left(\frac{\theta}{2}\right) - \frac{\theta^2}{8}\csc^2\left(\frac{\theta}{2}\right),\\ \theta^2 b(\theta) &= 1 - \frac{1}{4}\theta\cot\left(\frac{\theta}{2}\right) - \frac{\theta^2}{8}\csc^2\left(\frac{\theta}{2}\right).\end{aligned} \tag{23}$$

Since $\eta = [\Theta^T, \beta^T]^T \in \mathbb{R}^6$ is presented before, here $\theta = \|\Theta\|$. Note that η is not uniquely defined when $\|\Theta\|$ is exactly π rad.

The relative acceleration $\dot{\tilde{\xi}}$ can be written as

$$\dot{\tilde{\xi}} = \dot{\xi} + \mathrm{ad}_\xi \mathrm{Ad}_{h-1}\xi^0 - \mathrm{Ad}_{h-1}\dot{\xi}^0. \tag{24}$$

Substituting the follower's dynamics equation (12) into (24) yields the relative acceleration as

$$\mathbb{I}\dot{\tilde{\xi}} = \mathrm{ad}_\xi^* \mathbb{I}\xi + \mathbb{I}\left(\mathrm{ad}_\xi \mathrm{Ad}_{h-1}\xi^0 - \mathrm{Ad}_{h-1}\dot{\xi}^0\right) + \tau_g + \tau_c + \tau_d. \tag{25}$$

Therefore, the coupled translational and rotational error tracking system is composed of the relative kinematics expressed by exponential coordinate (21) and the relative acceleration equation (25).

3. Adaptive Fixed-Time Terminal Sliding Mode Controller Design

This section proposes a novel fixed-time convergence adaptive control scheme inspired by the asymptotic convergence one. Some assumptions, definitions, and lemmas are given before proposing the controller.

3.1. Assumptions, Definitions, and Lemmas

Assumption 1. Assuming that the external disturbance T_d and F_d are constrained by some known constant $\tau_{cs} \in \mathbb{R}^6$, i.e., each component of τ_d must satisfy the following inequality:

$$\left|\tau_{d_i}\right| \le \tau_{cs_i}. \tag{26}$$

Assumption 2. Assume that the configuration (g^0 and g) and velocities (ξ^0 and ξ) of the two spacecrafts can be obtained for designing the controller for the follower spacecraft through onboard navigation devices.

Assumption 3. Each component of the control inputs is bounded by specified saturation values, expressed as follows:

$$\begin{aligned}\left|\tau_{c_i}\right| &\le T_{c_{\max}}, \quad i = 1, 2, 3,\\ \left|\tau_{c_i}\right| &\le F_{c_{\max}}, \quad i = 4, 5, 6.\end{aligned} \tag{27}$$

Assumption 4. The control inputs strictly dominate the unknown disturbance, given by

$$\begin{aligned}\left|\tau_{d_i}(t)\right| &\le T_{d\ \max} < T_{c_{\max}}, \quad i = 1, 2, 3,\\ \left|\tau_{d_i}(t)\right| &\le F_{d\ \max} < F_{c_{\max}}, \quad i = 4, 5, 6.\end{aligned} \tag{28}$$

Lemma 5. *For any $x \in \mathbb{R}^n$, $a \in \mathbb{R}$, the following equations hold:*

$$\begin{aligned}\frac{d|x|^{a+1}}{dt} &= (a+1)\ \mathrm{diag}\ (sig(x)^a)\dot{x},\\ \frac{dsig|x|^{a+1}}{dt} &= (a+1)\ \mathrm{diag}\ (|x|^a)\dot{x}.\end{aligned} \tag{29}$$

Definition 6. Considering a nonlinear system represented by the following differential equation:

$$\dot{x}(t) = f(x(t)), \quad x(0) = 0, f(0) = 0, \tag{30}$$

where $x \in \mathbb{R}^n$. The origin of (30) is said to be a finite-time stable equilibrium point if there exists $T(x)$ that satisfies $x(t) \equiv 0, \forall t > T(x)$.

Definition 7. Considering the system of differential equation (30): if the origin of (30) is globally finite-time stable with bounded settling time function $T(x_0)$, that is, $\exists T_{\max} > 0$ such that $T(x_0) < T_{\max}$. We conclude that it is a fixed-time stable equilibrium point. In other words, the convergence time of a fixed-time stable system is independent of the initial states of the system.

Lemma 8 [16]. *For $x_i \in \mathbb{R}$, $i = 1, 2, \cdots, n$, $0 < r_1 \le 1$, $r_2 > 1$, the following inequalities hold:*

$$\begin{aligned}\left(\sum_{i=1}^n |x_i|\right)^{r_1} &\le \sum_{i=1}^n |x_i|^{r_1},\\ \left(\sum_{i=1}^n |x_i|\right)^{r_2} &\le n^{r_2-1}\sum_{i=1}^n |x_i|^{r_2}.\end{aligned} \tag{31}$$

Lemma 9 [39]. *Assuming that $V(t)$ is a continuous positive definite function and satisfies the inequality as follows:*

$$\dot{V}(t) + \lambda_1 V(t) + \lambda_2 V^{\sigma}(t) \le 0, \quad \forall t > 0, \tag{32}$$

we conclude that $V(t)$ will converge to the equilibrium point in finite time bounded by

$$T \le \frac{1}{\lambda_1(1-\sigma)} \ln \frac{\lambda_1 V^{1-\sigma}(t_0) + \lambda_2}{\lambda_2}, \tag{33}$$

where $\lambda_1 > 0, \lambda_2 > 0$ and $0 < \sigma < 1$.

Lemma 10 [40]. *Assuming that $V(t)$ is a continuous positive definite function and satisfies the inequality as follows:*

$$\dot{V}(t) + \lambda_1 V(t)^{\sigma_2} + \lambda_2 V(t)^{\sigma_2} \le 0, \quad \forall t > 0, \tag{34}$$

where $\lambda_1 > 0, \lambda_2 > 0$ and $1 < \sigma_1 < \infty, 0 < \sigma_2 < 1$, we conclude that $V(t)$ will converge to the equilibrium point in fixed time bounded by

$$T \le \frac{1}{\lambda_1(\sigma_1 - 1)} + \frac{1}{\lambda_2(1-\sigma_2)}. \tag{35}$$

Lemma 11 [41]. *Assuming that $V(t)$ is a continuous positive definite function and satisfies the inequality as follows:*

$$\begin{aligned} \dot{V}(t) + \lambda_1 V(t)^{(1/2)+(1/2)\sigma_1+((1/2)\sigma_1-(1/2))\ \mathrm{sgn}\ (V(t)-1)} \\ + \lambda_2 V(t)^{\sigma_2} \le 0, \quad \forall t > 0, \end{aligned} \tag{36}$$

where $\lambda_1 > 0, \lambda_2 > 0$ and $1 < \sigma_1 < \infty, 0 < \sigma_2 < 1$, we conclude that $V(t)$ will converge to the equilibrium point in fixed time bounded by

$$T \le \frac{1}{\lambda_1(\sigma_1 - 1)} + \frac{1}{\lambda_1(1-\sigma_2)} \ln\left(1 + \frac{\lambda_1}{\lambda_2}\right). \tag{37}$$

Since the inequality $\ln(1 + (\lambda_1/\lambda_2)) \le (\lambda_1/\lambda_2)$ holds, the convergence time proposed in Lemma 11 is shorter than that in Lemma 10.

3.2. Fixed-Time Terminal Sliding Mode Surface. The fixed-time type sliding surface consists of exponential coordinate of configuration tracking error and relative velocity tracking error, and is defined as:

$$s = \tilde{\xi} + C_1 \mathrm{sig}(\tilde{\eta})^{\sigma_1} + C_2 \mathrm{sig}(\tilde{\eta})^{\sigma_2}, \tag{38}$$

where $s = [s_1, \cdots, s_6]^T \in \mathbb{R}^6$ is the sliding surface, $\tilde{\xi} = [\xi_1, \cdots \xi_{6,}]^T$, $\mathrm{sig}(\tilde{\eta})^{\sigma} = [\mathrm{sig}(\eta)_1^{\sigma}, \cdots, \mathrm{sig}(\eta)_6^{\sigma_1}]^T$, $C_1 = \mathrm{diag}\ (c_{11}, \cdots, c_{16})$ and $C_2 = \mathrm{diag}\ (c_{21}, \cdots, c_{26})$ are both positive definite matrices, and $1 < \sigma_1 < \infty, 0 < \sigma_2 < 1$.

3.3. Adaptive Controller. Inspired by Ref. [6], the main results of this research are the adaptive finite-time and fixed-time control laws for spacecraft 6-DOF tracking maneuver. The adaptive control laws need no information about the inertia parameters and disturbances. In addition, it does not need to know the bounds of the eigenvalues of the inertia matrix and mass. The following theorem will propose an adaptive fixed-time type controller. Moreover, it will be proved that the controller guarantees the rotational and translational tracking errors to converge to the equilibrium points in fixed time.

To design a fixed-time terminal sliding mode control law, an adaptive fixed-time TSM-type reaching law is defined as [41]

$$\dot{s}(t) = -K_{s1} \mathrm{sig}(s)^{\sigma_1} - K_{s2} \mathrm{sig}(s)^{\sigma_1}, \tag{39}$$

where K_{s1} and K_{s1} are both positive definite matrices. The reaching law-based control scheme is able to ensure stabilization of a closed-loop system. By tuning the coefficient matrices K_{s1} and K_{s1}, chattering will be attenuated.

Considering the error tracking kinematics and dynamics shown in (21) and (25), respectively, the unified feedback control law is given as follows (named as AFixed in abbreviation):

$$\begin{aligned} \tau_c = -\Big(\hat{\tau}_g + \hat{\tau}_d + \mathrm{ad}_{\xi}^{*}\hat{\mathbb{I}}\xi + \hat{\mathbb{I}}\Big(\mathrm{ad}_{\xi}\mathrm{ad}_{h-1}\xi^0 - \mathrm{ad}_{h-1}\dot{\xi}^0 \\ + \Lambda_1 G(\tilde{\eta})\tilde{\xi} + \Lambda_2 G(\tilde{\eta})\tilde{\xi}\Big)\Big) - K_{s1}\mathrm{sig}(s)^{\sigma_1} \\ - K_{s2}\mathrm{sig}(s)^{\sigma_2} - K_g G^T(\tilde{\eta})\tilde{\eta}, \end{aligned} \tag{40}$$

where

$$s = \tilde{\xi} + C_1 \mathrm{sig}(\tilde{\eta})^{\sigma_1} + C_2 \mathrm{sig}(\tilde{\eta})^{\sigma_2}, \tag{41}$$

$$\Lambda_1 = \mathrm{diag}\ \left(\sigma_1 C_1 |\tilde{\eta}|^{\sigma_1 - 1}\right), \tag{42}$$

$$\Lambda_2 = \mathrm{diag}\ \left(\sigma_2 C_2 |\tilde{\eta}|^{\sigma_2 - 1}\right). \tag{43}$$

$\hat{\tau}_g$ is the estimated unified gravity force vector denoted as follows which takes a same form as previous:

$$\begin{aligned} \hat{\tau}_g &= \begin{bmatrix} \hat{M}_g \\ \hat{F}_g + \hat{m} R^T a_{J_2} \end{bmatrix}, \\ \hat{M}_g &= 3\left(\frac{\mu}{\|p\|^5}\right)\left(\left[b^{\times}\right]\hat{J}b\right), \\ \hat{F}_g &= -\left(\frac{\hat{m}\mu}{\|p\|^3}\right)b. \end{aligned} \tag{44}$$

$\hat{\mathbb{I}}$ is an estimated vector of the inertia parameters and updated by the following equation:

$$\begin{aligned} \frac{d}{dt}\nu(\hat{\mathbb{I}}) = K_i h\Big(s, \mathrm{ad}_{\xi}\mathrm{ad}_{h-1}\xi^0 - \mathrm{ad}_{h-1}\dot{\xi}^0 + \Lambda_1 G(\tilde{\eta})\tilde{\xi} + \Lambda_2 G(\tilde{\eta})\tilde{\xi} \\ + a_{gE} + a_{J_2 E}\Big) - K_i\Big(h(ad_s\xi, \xi) + h\big(\mathrm{ad}_s b_{\mu E}, b_E\big)\Big), \end{aligned} \tag{45}$$

where $K_i \in \mathbb{R}^{6\times6}$ is a positive definite matrix, $a_{gE} = [0_{1\times3}, -(\mu b^T/\|p\|^3)]^T$, $a_{J_2E} = [0_{1\times3}, a_{J_2}^T R]^T$, $b_{\mu E} = [(3\mu b^T/\|p\|^5), 0_{1\times3}]^T$, $b_E = [b^T, 0_{1\times3}]^T$, and $v(\mathbb{I}) = [J_{11}, J_{12}, J_{13}, J_{22}, J_{23}, J_{33}, m]^T$ is a vectorized version of the inertia matrix $\mathbb{I}$; the function $h(\cdot,\cdot)$ is defined as $a^T\mathbb{I}b = h(a,b)^T v(\mathbb{I}) = v(\mathbb{I})^T h(a,b)$,

$$h(a,b) = [a_1b_1, a_2b_1 + a_1b_2, a_3b_1 + a_1b_3, a_2b_2, a_3b_2 + a_2b_3, a_4b_4 + a_5b_5 + a_6b_6]^T, \tag{46}$$

where $\hat{\tau}_d$ is the disturbance estimations updated by

$$\frac{d}{dt}\hat{\tau}_d = K_{js}, \tag{47}$$

where $K_j \in \mathbb{R}^{6\times6}$ is a positive definite matrix.

Theorem 12. *Under Assumption 1 and Assumption 3, we apply the proposed control law (40) and the adaptive update laws (45) and (47) to the 6-DOF-coupled relative dynamics model. Then the S_i will converge to region $S_i \le O_s$ in fixed time. Also the tracking error $\tilde{\xi}$ and $\tilde{\eta}$ will converge into the regions $|\tilde{\xi}_i| \le O_{\tilde{\xi}}$ and $|\tilde{\eta}_i| \le O_{\tilde{\eta}}$ in fixed time, respectively.*

$$\begin{aligned}
O_s &= \min\left(\sqrt{\frac{2}{\lambda_{\min}(\mathbb{I})}}\left(\frac{\Delta'}{\kappa_1}\right)^{1/1+\sigma_1}, \sqrt{\frac{2}{\lambda_{\min}(\mathbb{I})}}\left(\frac{\Delta'}{\kappa_2}\right)^{1/1+\sigma_2}\right),\\
O_{\tilde{\eta}} &= \min\left(\sqrt[\sigma 1]{\frac{O_s}{\lambda_{\min}(C_1)}}, \sqrt[\sigma 2]{\frac{O_s}{\lambda_{\min}(C_2)}}\right),\\
O_{\tilde{\xi}} &= O_s + \lambda_{\max}(C_1)O_{\tilde{\eta}}^{\sigma_1} + \lambda_{\max}(C_2)O_{\tilde{\eta}}^{\sigma_2},
\end{aligned} \tag{48}$$

where $\lambda_{\min}(\cdot)$ and $\lambda_{\max}(\cdot)$ denote the minimum and maximum eigenvalues of a matrix, respectively. S_i denotes the ith component of s.

Proof. Step 1. This step proves that a certain component of sliding surface S_i will converge to the region O_s in fixed time that satisfying $S_i \le O_s$.

First, the inertia matrix (consists of the moment of inertia matrix and mass) and external disturbance estimated errors are defined as

$$\begin{aligned}
\tilde{\mathbb{I}} &= \hat{\mathbb{I}} - \mathbb{I},\\
\tilde{\tau}_d &= \hat{\tau}_d - \tau_d.
\end{aligned} \tag{49}$$

Note that $\tilde{\eta} = 0_{6\times1}$, $s = 0_{6\times1}$, $v(\tilde{\mathbb{I}}) = 0_{7\times1}$, and $\tilde{\tau}_d = 0_{6\times1}$ are the equilibrium points of the closed-loop system represented by equation (9). A candidate Lyapunov function is designed as follows:

$$V\left(\tilde{\eta}, s, v\left(\tilde{\mathbb{I}}\right), \tilde{\tau}_d\right) = \frac{1}{2}\tilde{\eta}^T K_g\tilde{\eta} + \frac{1}{2}s^T\mathbb{I}s + \frac{1}{2}v\left(\tilde{\mathbb{I}}\right)^T K_i^{-1}v\left(\tilde{\mathbb{I}}\right) + \frac{1}{2}\tilde{\tau}_d^T K_j^{-1}\tilde{\tau}_d. \tag{50}$$

V is said to be a valid Lyapunov function since $V(\tilde{\eta} = 0, s = 0, v(\tilde{\mathbb{I}}) = 0, \tilde{\tau}_d = 0) = 0$ and $V(\tilde{\eta}, s, v(\tilde{\mathbb{I}}), \tilde{\tau}_d) > 0$, for all $(\tilde{\eta} = 0, s = 0, v(\tilde{\mathbb{I}}) = 0, \tilde{\tau}_d = 0) \in \mathbb{R}^6\times\mathbb{R}^6\times\mathbb{R}^7\times\mathbb{R}^6\{0_{6\times1}, 0_{6\times1}, 0_{7\times1}, 0_{6\times1}\}$. Taking the derivative of V yields

$$\dot{V} = \tilde{\eta}^T K_g\dot{\tilde{\eta}} + s^T\mathbb{I}\dot{s} + v\left(\tilde{\mathbb{I}}\right)^T K_i^{-1}\dot{v}\left(\tilde{\mathbb{I}}\right) + \tilde{\tau}_d^T K_j^{-1}\dot{\tilde{\tau}}_d. \tag{51}$$

According to equations (21) and (41), we have $G(\tilde{\eta})s = G(\tilde{\eta})\tilde{\xi} + G(\tilde{\eta})C_1 sig(\tilde{\eta})^{\sigma_1} + G(\tilde{\eta})C_2 sig(\tilde{\eta})^{\sigma_2}$, then

$$\dot{\tilde{\eta}} = G(\tilde{\eta})\tilde{\xi} = G(\tilde{\eta})s - G(\tilde{\eta})C_1 sig(\tilde{\eta})^{\sigma_1} - G(\tilde{\eta})C_2 sig(\tilde{\eta})^{\sigma_2}. \tag{52}$$

Taking the time derivative of the sliding mode surface (41), together with equation (52), then plug them into $\dot{V}$ yields

$$\begin{aligned}
\dot{V} = {}& \tilde{\eta}^T K_g(G(\tilde{\eta})s - G(\tilde{\eta})C_1 sig(\tilde{\eta})^{\sigma_1} - G(\tilde{\eta})C_2 sig(\tilde{\eta})^{\sigma_2})\\
&+ s^T\mathbb{I}\dot{\tilde{\xi}} + s^T\mathbb{I}\left(\Lambda_1\dot{\tilde{\eta}} + \Lambda_2\dot{\tilde{\eta}}\right) + v\left(\tilde{\mathbb{I}}\right)^T K_i^{-1}\dot{v}\left(\tilde{\mathbb{I}}\right) + \tilde{\tau}_d^T K_j^{-1}\dot{\tilde{\tau}}_d.
\end{aligned} \tag{53}$$

Applying equations (21) and (25) to the above equation,

$$\begin{aligned}
\dot{V} = {}& \tilde{\eta}^T K_g G(\tilde{\eta})s - \tilde{\eta}^T K_g G(\tilde{\eta})C_1\tilde{\eta}^{\sigma_1} - \tilde{\eta}^T K_g G(\tilde{\eta})C_2\tilde{\eta}^{\sigma_2}\\
&+ s^T\left(\mathrm{ad}_{\tilde{\xi}}^*\mathbb{I}\xi + \tau_g + \tau_c + \tau_d + \mathbb{I}\left(\mathrm{ad}_{\xi}\mathrm{ad}_{h-1}\xi^0 - \mathrm{ad}_{h-1}\dot{\xi}^0\right.\right.\\
&\left.\left.+ \Lambda_1\dot{\tilde{\eta}} + \Lambda_2\dot{\tilde{\eta}}\right)\right) + v\left(\tilde{\mathbb{I}}\right)^T K_i^{-1}\dot{v}\left(\tilde{\mathbb{I}}\right) + \tilde{\tau}_d^T K_j^{-1}\dot{\tilde{\tau}}_d.
\end{aligned} \tag{54}$$

Plugging the feedback control law (40) yields

$$\begin{aligned}
\dot{V} = {}& \tilde{\eta}^T K_g G(\tilde{\eta})s - \tilde{\eta}^T K_g G(\tilde{\eta})C_1\tilde{\eta}^{\sigma_1} - \tilde{\eta}^T K_g G(\tilde{\eta})C_2\tilde{\eta}^{\sigma_2}\\
&- s^T\left(\mathrm{ad}_{\tilde{\xi}}^*\tilde{\mathbb{I}}\xi + \tilde{\tau}_g + \tilde{\tau}_d + \tilde{\mathbb{I}}\left(\mathrm{ad}_{\tilde{\xi}}\mathrm{ad}_{h-1}\xi^0 - \mathrm{ad}_{h-1}\dot{\xi}^0\right.\right.\\
&\left.\left.+ \Lambda_1\dot{\tilde{\eta}} + \Lambda_2\dot{\tilde{\eta}}\right)\right) - s^T\left(K_{s1}sig(s)^{\sigma_1} + K_{s2}sig(s)^{\sigma_2}\right.\\
&\left.+ K_g G^T(\tilde{\eta})\tilde{\eta}\right) + v\left(\tilde{\mathbb{I}}\right)^T K_i^{-1}\dot{v}\left(\tilde{\mathbb{I}}\right) + \tilde{\tau}_d^T K_j^{-1}\dot{\tilde{\tau}}_d.
\end{aligned} \tag{55}$$

Since $\dot{v}(\tilde{\mathbb{I}})$ and $\dot{\tilde{\tau}}$ are defined by equations (45) and (47), respectively, it shows that

$$\begin{aligned}
\dot{V} = {}& -\tilde{\eta}^T K_g G(\tilde{\eta})C_1\mathrm{sig}(\tilde{\eta})^{\sigma_1} - \tilde{\eta}^T K_g G(\tilde{\eta})C_2\mathrm{sig}(\tilde{\eta})^{\sigma_2}\\
&- s^T K_{s1}\mathrm{sig}(s)^{\sigma_1} - s^T K_{s2}\mathrm{sig}(s)^{\sigma_2}.
\end{aligned} \tag{56}$$

According to Lemma 8, the following inequality holds:

$$\begin{aligned}\dot{V} \le & -6^{1-\sigma_1/2}\lambda_{\min}\left(\frac{2}{\lambda_{\max}(\mathbb{I})}\right)^{1-\sigma_1/2}\left(\frac{1}{2}s^T\mathbb{I}s\right)^{1-\sigma_1/2} \\ & -\lambda_{\min}(K_{s2})\left(\frac{2}{\lambda_{\max}(\mathbb{I})}\right)^{1-\sigma_2/2}\left(\frac{1}{2}s^T\mathbb{I}s\right)^{1-\sigma_2/2} \\ & -6^{1-\sigma_1/2}\lambda_{\min}(GC_1)2^{1-\sigma_1/2}\left(\frac{1}{2}\tilde{\eta}^TK_g\tilde{\eta}\right)^{1-\sigma_1/2} \\ & -\lambda_{\min}(GC_2)2^{1-\sigma_2/2}\left(\frac{1}{2}\tilde{\eta}^TK_g\tilde{\eta}\right)^{1-\sigma_2/2}.\end{aligned} \tag{57}$$

Considering the last two terms of $\dot{V}$

$$\begin{aligned}\dot{V} \le & -6^{(1-\sigma_1)/2}\lambda_{\min}(K_{s1})\left(\frac{2}{\lambda_{\max}(\mathbb{I})}\right)^{(1+\sigma_1)/2}\left(\frac{1}{2}s^T\mathbb{I}s\right)^{(1+\sigma_1)/2} \\ & -\lambda_{\min}(K_{s2})\left(\frac{2}{\lambda_{\max}(\mathbb{I})}\right)^{(1+\sigma_2)/2}\left(\frac{1}{2}s^T\mathbb{I}s\right)^{(1+\sigma_2)/2} \\ & -6^{(1-\sigma_1)/2}\lambda_{\min}(GC_1)2^{(1+\sigma_1)/2}\left(\frac{1}{2}\tilde{\eta}^TK_g\tilde{\eta}\right)^{(1+\sigma_1)/2} \\ & -\lambda_{\min}(GC_2)2^{(1+\sigma_2)/2}\left(\frac{1}{2}\tilde{\eta}^TK_g\tilde{\eta}\right)^{(1+\sigma_2)/2} \\ & -\left(\frac{1}{2}\nu\left(\tilde{\mathbb{I}}\right)^TK_i^{-1}\nu\left(\tilde{\mathbb{I}}\right)\right)^{(1+\sigma_1)/2}-\left(\frac{1}{2}\nu\left(\tilde{\mathbb{I}}\right)^TK_i^{-1}\nu\left(\tilde{\mathbb{I}}\right)\right)^{(1+\sigma_2)/2} \\ & -\left(\frac{1}{2}\tilde{\tau}_d^TK_j^{-1}\tilde{\tau}_d\right)^{(1+\sigma_1)/2}-\left(\frac{1}{2}\tilde{\tau}_d^TK_j^{-1}\tilde{\tau}_d\right)^{(1+\sigma_2)/2}+\Delta,\end{aligned} \tag{58}$$

where Δ is defined as

$$\begin{aligned}\Delta = & \left(\frac{1}{2}\nu\left(\tilde{\mathbb{I}}\right)^TK_i^{-1}\nu\left(\tilde{\mathbb{I}}\right)\right)^{1+\sigma_1/2}+\left(\frac{1}{2}\nu\left(\tilde{\mathbb{I}}\right)^TK_i^{-1}\nu\left(\tilde{\mathbb{I}}\right)\right)^{1+\sigma_2/2} \\ & +\left(\frac{1}{2}\tilde{\tau}_d^TK_j^{-1}\tilde{\tau}_d\right)^{1+\sigma_1/2}+\left(\frac{1}{2}\tilde{\tau}_d^TK_j^{-1}\tilde{\tau}_d\right)^{1+\sigma_2/2}.\end{aligned} \tag{59}$$

Assuming that there exist unknown constants χ_1, χ_2 satisfying $\|\nu(\tilde{\mathbb{I}})\| \le \chi_1$ and $\|\tilde{\tau}_d\| \le \chi_2$, respectively. Then Δ satisfies the following inequality

$$\begin{aligned}\Delta \le & \left(\frac{1}{2}\lambda_{\max}\left(K_i^{-1}\right)\chi_1^2\right)^{1+\sigma_1/2}+\left(\frac{1}{2}\lambda_{\max}\left(K_i^{-1}\right)\chi_1^2\right)^{1+\sigma_2/2} \\ & +\left(\frac{1}{2}\lambda_{\max}\left(K_j^{-1}\right)\chi_2^2\right)^{1+\sigma_1/2}+\left(\frac{1}{2}\lambda_{\max}\left(K_j\right)\chi_1^2\right)^{1+\sigma_2/2}=\Delta'.\end{aligned} \tag{60}$$

It is obvious that Δ' is bounded. We define κ_1, κ_1, as follows:

$$\begin{aligned}\kappa_1 = & 4^{1-\sigma_1/2}\min\left(-6^{1-\sigma_1/2}\lambda_{\min}(K_{s1})\left(\frac{2}{\lambda_{\max}(\mathbb{I})}\right)^{1+\sigma_1/2},\right. \\ & \left.-6^{1-\sigma_1/2}\lambda_{\min}(GC_1)2^{1+\sigma_1/2},1\right),\end{aligned}$$

$$\kappa_2 = \min\left(\lambda_{\min}(K_{s2})\left(\frac{2}{\lambda_{\max}(\mathbb{I})}\right)^{1+\sigma_2/2},\lambda_{\min}(GC_2)2^{1+\sigma_2/2},1\right). \tag{61}$$

Then the inequality (58) can be simplified as

$$\dot{V} \le -\kappa_1V^{1+\sigma_1/2}-\kappa_2V^{1+\sigma_2/2}+\Delta'. \tag{62}$$

Hence V will converge into the region $O_V = \min\left(\left(\Delta'/\kappa_1\right)^{2/1+\sigma_1}, \left(\Delta'/\kappa_2\right)^{2/1+\sigma_2}\right)$ in fixed time.

The following inequalities hold:

$$\begin{aligned}\frac{1}{2}s^T\mathbb{I}s \le V, \\ \frac{1}{2}\tilde{\eta}^TK_g\tilde{\eta} \le V.\end{aligned} \tag{63}$$

Then we can conclude that $|S_i|$ will converge to the region $O_s = \sqrt{(2/\lambda_{\min}(\mathbb{I}))O_V}$ in fixed time and $|\eta_i|$ will converge to $O_{\tilde{\eta}} = \sqrt{(2/\lambda_{\min}(K_g))O_V}$ simultaneously.

Step 2. In this step, we prove that the tracking errors $\tilde{\xi}_i$ and $\tilde{\eta}_i$ will converge into the small regions $O_{\tilde{\xi}}$ and $O_{\tilde{\eta}}$ in fixed time, respectively. Then, for $|S_i| \le O_s$ in Step 1, it follows the two cases given as follows:

Case 1. If $S_i = 0$ is reached, $\tilde{\xi}_i = 0 \in O_{\tilde{\xi}}$ and $\tilde{\eta}_i = 0 \in O_{\tilde{\eta}}$ will be reached in fixed time according to Lemma 10.

Case 2. If $S_i \ne 0$, according to the sliding surface, it means that the tracking error1 $\tilde{\eta}_i$ has converged into the region $\tilde{\eta}_i \le O_{\tilde{\eta}}$. Based on equation (38), we have $\tilde{\xi}_i + C_{1i}\mathrm{sig}(\tilde{\eta}_i)^{\sigma_1} + C_{2i}\mathrm{sig}(\tilde{\eta}_i)^{\sigma_2} = \psi_i$, $|\psi_i| \le O_s$. It follows that $|\tilde{\xi}_i| \le |\psi_i| + C_{1i}\mathrm{sig}(\tilde{\eta}_i)^{\sigma_1} + C_{2i}\mathrm{sig}(\tilde{\eta}_i)^{\sigma_2} \le O_{\tilde{\xi}}$. This inequality shows that $\tilde{\eta}_i$ has converged into the region $|\tilde{\xi}_i| \le O_{\tilde{\xi}}$. According to Lemma 10, we can conclude that the tracking errors $\tilde{\eta}_i$ and $\tilde{\xi}_i$ will converge to the regions $|\tilde{\eta}_i| \le O_{\tilde{\eta}}$ and $|\tilde{\xi}_i| \le O_{\tilde{\xi}}$ in fixed time, respectively.

3.4. Other Sliding Surfaces and Reaching Laws. If the power σ_1 in sliding surface (38) and reaching law (39) is replaced by a power that takes the form as

$$\frac{1}{2}+\frac{1}{2}\sigma_1\left(\frac{1}{2}\sigma_1-\frac{1}{2}\right)\operatorname{sgn}(|x|-1), \tag{64}$$

i.e., when $|s_i|<1$ in the reaching phase and $|\tilde{\eta}_i|<1$ in the sliding phase are satisfied, the power σ_1 switches to 1. According to Lemma 11, the modified power will lead to a faster convergence rate. To compare different controllers' performances, we present the following sliding surfaces and reaching laws, as well as the corresponding control laws.

(i) Adaptive fixed-time terminal sliding mode control law (AFixed): the corresponding sliding surface (38), reaching law (39), and control law (40) are presented previously

(ii) Adaptive modified fixed-time terminal sliding mode control law (AMFixed):

$$s=\tilde{\xi}+C_1\operatorname{sig}(\tilde{\eta})^{1/2+1/2\sigma_1+((1/2)\sigma_1-(1/2))\operatorname{sign}(|\tilde{\eta}|-1)}+C_2\operatorname{sig}(\tilde{\eta})^{\sigma_2}, \tag{65}$$

$$\dot{s}(t)=-K_{s1}\operatorname{sig}(s)^{1/2+1/2\sigma_1+((1/2)\sigma_1-(1/2))\operatorname{sign}(|s|-1)}-K_{s2}\operatorname{sig}(\tilde{s})^{\sigma_2}, \tag{66}$$

$$\begin{aligned}\tau_c=&-\Big(\hat{\tau}_g+\hat{\tau}_d+\operatorname{ad}^*_{\xi}\hat{\mathbb{I}}\xi+\hat{\mathbb{I}}\Big(\operatorname{ad}_{\xi}\operatorname{ad}_{h-1}\xi^0\\&-\operatorname{ad}_{h-1}\dot{\xi}^0+\Lambda_1G(\tilde{\eta})\tilde{\xi}+\Lambda_1G(\tilde{\eta})\tilde{\xi}\Big)\Big)\\&-\Big(K_{s1}\operatorname{sig}(s)^{1/2+1/2\sigma_1+((1/2)\sigma_1-(1/2))\operatorname{sign}(|s|-1)}\\&+K_{s2}\operatorname{sig}(s)^{\sigma_2}+K_gG^T(\tilde{\eta})\tilde{\eta}\Big)\end{aligned} \tag{67}$$

(iii) Adaptive finite-time terminal sliding mode control law (AFinite):

$$s=\tilde{\xi}+C_1\tilde{\eta}+C_2\operatorname{sig}(\tilde{\eta})^{\sigma_2}, \tag{68}$$

$$\dot{s}(t)=-K_{s1}s-K_{s2}\operatorname{sig}(\tilde{s})^{\sigma_2}, \tag{69}$$

$$\begin{aligned}\tau_c=&-\Big(\hat{\tau}_g+\hat{\tau}_d+\operatorname{ad}^*_{\xi}\hat{\mathbb{I}}\xi+\hat{\mathbb{I}}\Big(\operatorname{ad}_{\xi}\operatorname{ad}_{h-1}\xi^0-\operatorname{ad}_{h-1}\dot{\xi}^0\\&+\Lambda_1G(\tilde{\eta})\tilde{\xi}+\Lambda_2G(\tilde{\eta})\tilde{\xi}\Big)\Big)-(K_{s1}s+K_{s2}\operatorname{sig}(s)^{\sigma_2}\\&+G^T(\tilde{\eta})\tilde{\eta})\end{aligned} \tag{70}$$

Let abbreviations AFixed, AMFixed, and AFinite represent the three controllers, respectively. Since the sliding surfaces and reaching laws have similar forms, the feedback control laws take similar forms as equation (40). The convergence properties of the feedback control laws are easy to prove and the proofs will not go into details here. In the simulation section, different feedback control laws will be applied to the error tracking control system.

The proposed control laws and adaptive update laws take similar forms as ones in Ref. [6]. As extensions of adaptive control law with asymptotic convergence property proposed in Ref. [6], this study proposes fixed-time and finite-time convergent adaptive control laws for 6-DOF tracking maneuver of a rigid body spacecraft. The control laws (40), (67), and (70) can be performed without accurate inertia parameters and information about external disturbances. Thus, the proposed control laws and update laws can be applied to the coupled spacecraft 6-DOF tracking system, although there exist large inertia parametric uncertainties and external disturbances.

Remark 13. In this study, the follower's states and the leader's states are simulated simultaneously. Kinematics equations of the two take the same forms as that of relative motion, which are

$$\dot{\eta}^0=G(\eta^0)\xi^0, \tag{71}$$

$$\dot{\eta}=G(\eta)\xi. \tag{72}$$

The leader's differential equations (71) and (15) and the follower's differential equations (12) and (72) can be integrated by the Runge-Kutta method which is suitable for the Euclidean space, since $\eta^0(t), \xi^0(t)$ and $\eta(t), \xi(t)$ are vectors in $\mathbb{R}^6$. Then the poses of the two spacecrafts are obtained through the exponential map from se(3) to SE(3). Thereafter, the relative states can be computed by using equations in the second section, which will be applied to the control laws.

4. Numerical Simulation Results

The initial states are given, and the proposed controllers are simulated in this section. The function blkdiag($M_1, M_2,\cdots, M_n$) in Table 1 denotes the block diagonal matrix composed of submatrices $(M_1, M_2,\cdots,M_n)$. The parameters in Table 1 satisfy the equalities: $C_1=C_2, K_{s1}=K_{s2}$. The three controllers for coupled spacecraft tracking maneuver are simulated, mainly to demonstrate the effectiveness of AMFixed (67). AMFixed will achieve better control performances theoretically according to Lemma 11. The other control laws, AFixed (40) and AFinite (70), are also applied to the closed-loop feedback system to compare their performances with AMFixed (67). The leader spacecraft moves on a Molniya orbit which would increase complexity to the maneuver task, and the follower moves on the neighboring orbit. Table 2 presents the leader's initial orbital elements, supposing that the leader's initial attitude is to align its body-fixed frame with its LVLH frame. The leader is assumed to move freely in the gravity field, and not be affected by any external disturbance or maneuver. The purpose of the control is to drive the actual relative states to the desired relative states by performing maneuvers. In other words, the follower spacecraft should achieve the desired relative pose h_d and keep the attitude in synchronizing with the leader. Here the desired position and velocity expressed in the leader's body-fixed frame are $[5\,0\,0]^T$ m and $[0\quad 0\quad 0]^T$ m/s, respectively. The initial relative position, attitude, and velocities

Table 1: Design parameters.

Design parameters	Values
σ_1, σ_2	5/4, 4/5
C_1, C_2	diag $(0.12, 0.12, 0.12, 0.084, 0.066, 0.063)$
K_{s1}, K_{s2}	blkdiag$(30I_3, 100I_3)$
K_i	blkdiag$(10^3 I_6, 2)$
K_j	$0.005I_6$
K_g	$0.1I_6$

Table 2: Initial orbital elements of the leader.

Orbital element	Value
Semimajor axis (km)	26628
Eccentricity	0.7417
Inclination (°)	63.4
Argument of perigee (°)	270
RAAN (°)	0
True anomaly (°)	120

are given in Table 3. The inertia parameters of the leader are defined as follows:

$$m^0 = 110\text{kg}, \quad J^0 = \begin{bmatrix} 21.7 & -0.2 & -0.5 \\ -0.2 & 22.3 & -0.3 \\ -0.5 & -0.3 & 25.5 \end{bmatrix} \text{kg} \cdot \text{m}^2. \tag{73}$$

The nominal inertia properties of the follower spacecraft are defined as follows:

$$m = 100\text{kg}, \quad J = \begin{bmatrix} 23.7 & -0.2 & -0.5 \\ -0.2 & 25.3 & -0.3 \\ -0.5 & -0.3 & 22.5 \end{bmatrix} \text{kg} \cdot \text{m}^2. \tag{74}$$

The follower spacecraft is assumed to be able to perform continuous control maneuvers. Constraints of control torque and force are denoted by $T_{c_i} \le T_{c\,\max} = 1\,\text{N} \cdot \text{m}$ and $F_{c_i} \le F_{c\,\max} = 10\,\text{N}$, respectively. The control parameters are presented in Table 1. The initial values of parameter estimations are chosen as $\widehat{\tau}_d(0) = [0, 0, 0, 0, 0, 0]^T$, $\nu(I(0)) = [0, 0, 0, 0, 0, 0, 0]^T$. The fourth-order Runge-Kutta method with MATLAB/SIMULINK is used for the numerical simulations. The step size is 0.01 s, and the simulation time is $t_f = 100$ s. Meanwhile, the external disturbances on the follower spacecraft are modeled as follows:

$T_d = 0.005[\sin(0.1t), \cos(0.1t), -\sin(0.1t)]^T$, $F_d = 0.05[\sin(0.1t), \cos(0.1t), -\sin(0.1t)]^T$. Figures 2 and 3 show

Table 3: Initial states of the follower spacecraft relative to the leader.

Initial states	Values
Leader's angular velocity (rad/s)	$[0, 0, 0.0011]^T$
Relative position (m)	$[15, 15, 15]^T$
Relative attitude (°)	120
Relative principal rotation axis	$[-2, -2, -3]^T$
Relative translational velocity (m/s)	$[-0.051, -0.247, -0.075]^T$
Relative angular velocity (rad/s)	$[0.009, 5.98, -9.31]^T \times 10^{-4}$

rotational and translational tracking errors, respectively. Here we describe the control performances of AMFixed in details. The magnitude of attitude tracking error $\tilde{\theta} = \|\tilde{\Theta}\|$ in Figure 2(a) converges to less than 0.0017° within 25 s, while the norm of the position tracking error $\tilde{\beta} = \|\tilde{\beta}(t)\|$ in Figure 3(a) corresponding to AMFixed converges to less than 0.028 m within 37 s. Figure 2(b) shows that the magnitude of angular velocity tracking error $\tilde{\omega}$ corresponding to AMFixed converges to less than $0.00061^\circ/s$ within 25 s, while Figure 3(b) shows that the magnitude of translational velocity tracking error $\tilde{\nu}$ corresponding to AMFixed converge to less than 0.0056 m/s within 37 s.

Figure 4(a) shows estimations of inertia parameters. It is observed that the inertia estimations are not exactly identified as their actual values. Because the control inputs in this case do not satisfy the persistent excitation condition. However, the adaptive control law does not need accurate values [42]. The disturbance estimations are shown in Figure 4(b), which also converge to constant values.

From the simulation results in Figures 2 and 3, we can know that attitude and position tracking errors of the three controllers are different. AMFixed and AFinite hold almost the same steady-state errors, and AFixed keeps the maximum steady-state errors in the three controllers. The convergence rates of the three controllers in attitude control are almost the same. When zooming in Figure 2(a), it can be found that the convergence rates of AMFixed and AFixed are slightly faster than that of AFinite in the midstage of attitude control. In Figure 3, it shows that position and velocity tracking errors of AMFixed and AFixed converge significantly faster than that of AFinite. The velocity tracking steady-state errors of the three controllers are almost the same.

Figure 5 shows control inputs (torques and forces) varying with time. Control torques and forces of the three control laws are shown in Figures 5(a) and 5(b), respectively. And each component of the control inputs is bounded by ±1 N·m (control torque) or ±10 N (control force), respectively. Control inputs on the follower spacecraft are saturate or relatively large in the early stage and then decrease quickly. The reaching law-based terminal sliding mode control laws in this study largely attenuate the chattering caused by the signum function-based sliding mode control. The performances of the three controllers are shown in Table 4. Let t_{st} in Table 4 denote the time to reach the steady state.

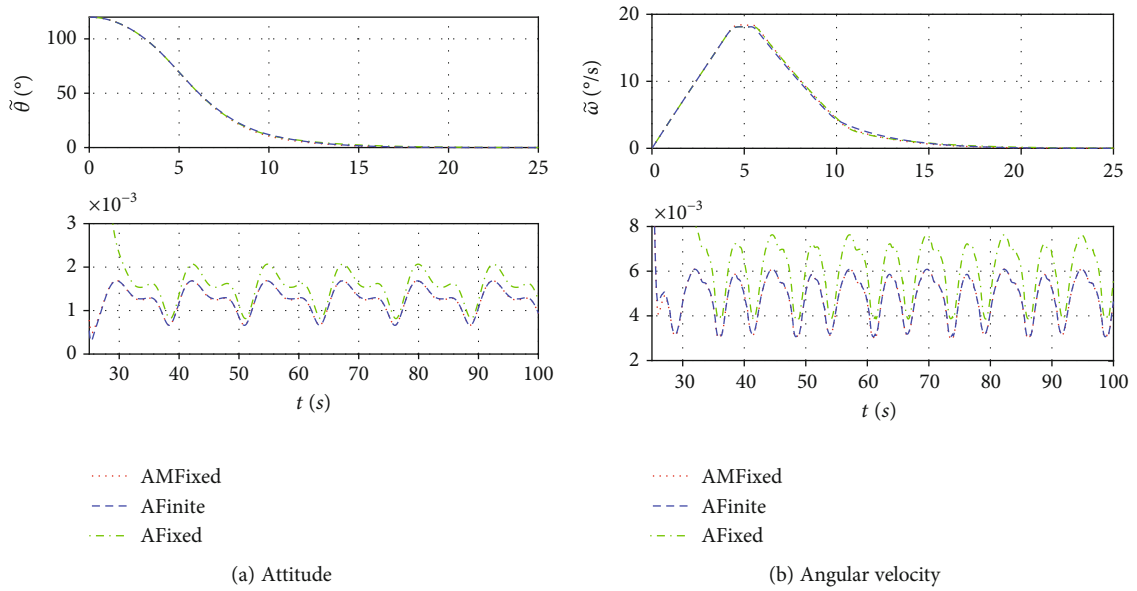

(a) Attitude (b) Angular velocity

Figure 2: Rotational tracking errors.

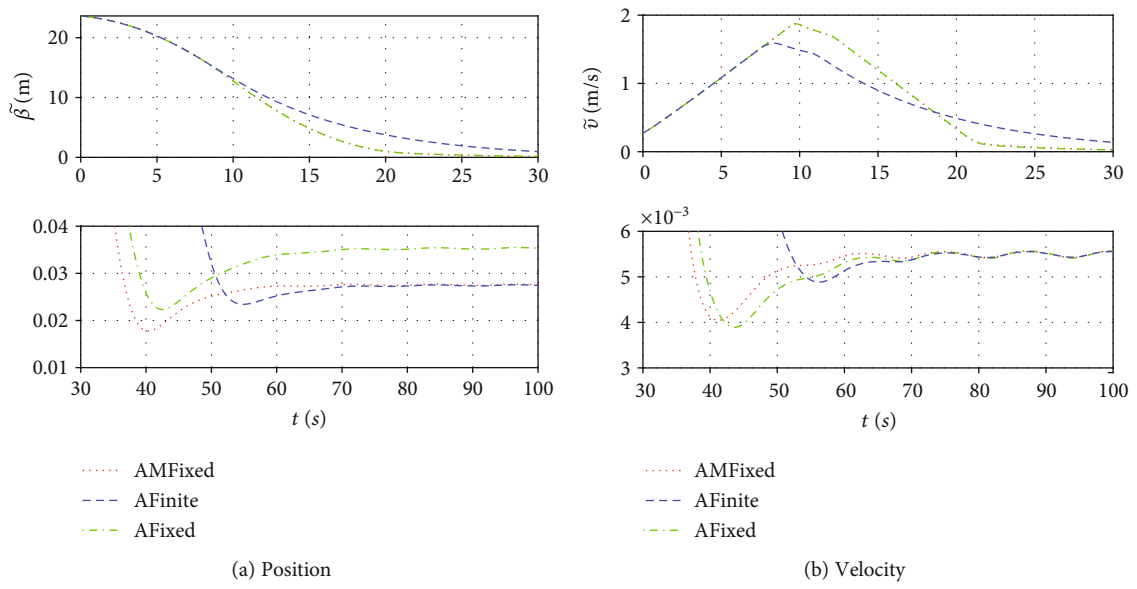

(a) Position (b) Velocity

Figure 3: Translational tracking errors.

From Figures 5 and 6, some evident features can be found. In attitude control processes of the three controllers, the control torque inputs varying with time are slightly different, while in position control processes of the three controllers, the control force inputs are quite different. In both attitude and position control processes, control inputs of AMFixed and AFixed decrease later than that of AFinite. The control force inputs of the two fixed-time control cases begin to decrease from about 20 s, and the control force inputs of the finite-time control case decrease from about 10 s. This is due to the power greater than 1 of the fixed-time control. Fixed-time control generates larger control inputs than the finite time control in the early stage. It means that the fixed-time control accelerates and brakes faster in the phase with relatively large error. The control torque effort (Integration of control torque) of AFinite is less than those AMFixed and AFixed, although the differences between them are small, while control force efforts (Integration of control force) of AFinite is significantly less than those of the other two. The faster accelerating and braking processes lead to more considerable control effort naturally. The difference between the three controllers is just the switching threshold with the magnitude of 1. The initial attitude error is relatively small compared to 1. This is the reason that the convergence

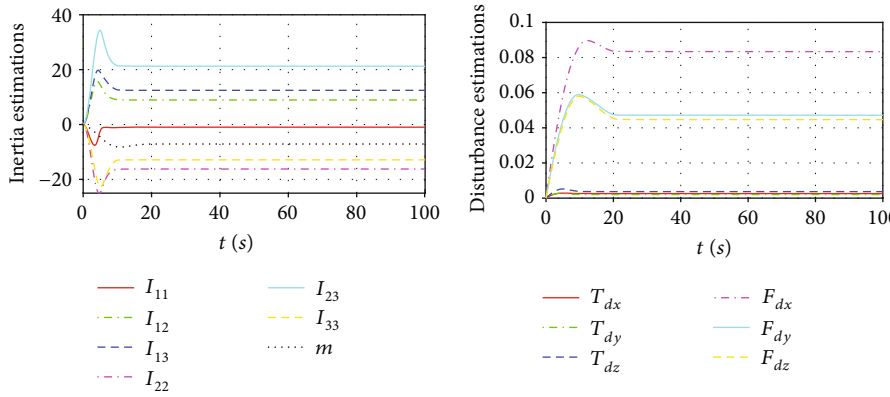

(a) Estimated inertia parameters (b) Estimated disturbances

Figure 4: Estimated parameters.

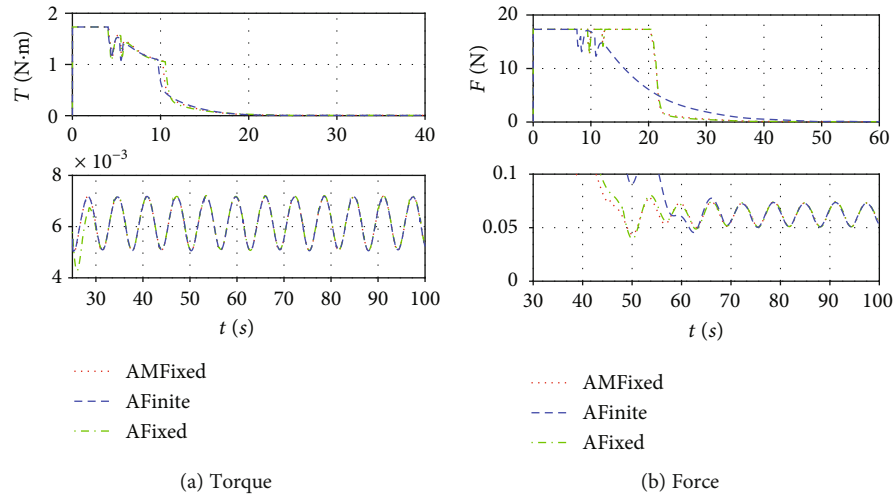

(a) Torque (b) Force

Figure 5: Control torque and force.

Table 4: Control performance comparisons.

Performance indices	AMFixed	AFixed	AFinite
$\left\|\tilde{\theta}(t_f)\right\|(^\circ)$	0.0017	0.002	0.0017
$\left\|\tilde{\beta}(t_f)\right\|(\mathrm{m})$	0.028	0.036	0.028
$\left\|\tilde{\omega}(t_f)\right\|(^\circ/\mathrm{s})$	0.00061	0.00077	0.0061
$\left\|\tilde{v}(t_f)\right\|(\mathrm{m/s})$	0.0056	0.0056	0.0056
$\int_0^{t_f} \|T_c\| dt(\mathrm{N\cdot s})$	16.95	16.95	16.66
$\int_0^{t_f} \|F_c\| dt(\mathrm{N\cdot m\cdot s})$	382.5	381.5	332
$t_{st}(\mathrm{s})(\mathrm{attitude})$	24.5	31	24.5
$t_{st}(\mathrm{s})(\mathrm{position})$	37	38	51

rates and control efforts of the three control laws hold just slight differences between each other in their attitude control processes.

In summary, the adaptive modified fixed-time control law (AMFixed) performs with higher control accuracy comparing to the conventional adaptive fixed-time control law (AFixed) and with faster convergence rate comparing to the adaptive finite-time control law (AFinite). These can be demonstrated clearly again in Table 4.

5. Conclusion

The control problem of spacecraft coupled rotational and translational maneuver tasks in the presence of large parametric uncertainties and external disturbances is studied. Based on the spacecraft relative coupled kinematics and dynamics equations on SE(3), a reaching law-based adaptive fixed-time terminal sliding mode control law and the modified one are designed. The two control laws are able to drive the states of the closed-loop feedback tacking system to converge to the equilibrium points in fixed time. The adaptive finite-time control law is proposed simultaneously to compare the control performances with each other. The states of the closed-loop system are almost globally convergent over the space $\mathrm{SE}(3) \times \mathbb{R}^6$. Numerical simulation results demonstrate

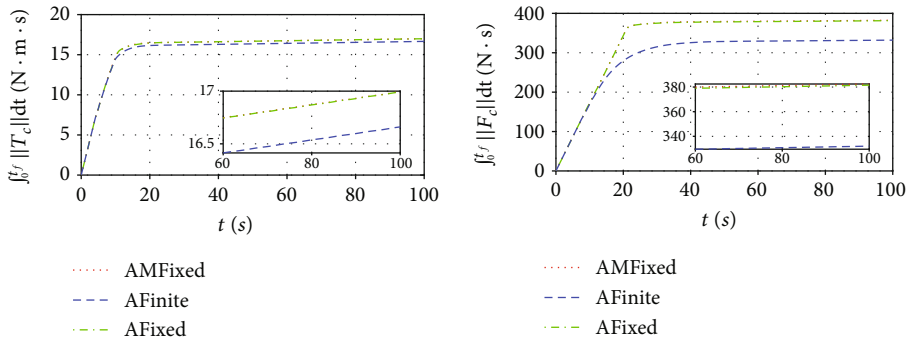

(a) Integration of control torque

(b) Integration of control force

FIGURE 6: Integration of control torque and force.

that the follower spacecraft can reach the desired pose and velocities in fixed time by applying proposed fixed-time control laws. Furthermore, it shows that the proposed adaptive modified fixed-time terminal sliding mode control law is superior to the conventional one with almost the same control effort. The two fixed-time type control laws drive the states with faster convergence rates than the finite-time one but cost more energy. There are some drawbacks related to the proposed inertia parameter update law and disturbance update law. The former cannot identify the actual inertia parameters when the persistent excitation condition is not satisfied. The latter cannot exactly identify the true external disturbances, and the estimations always converge to constant values.

Nomenclature

SO(3): Lie group of attitude matrix of the rigid body
SE(3): Lie group of attitude and positions of the rigid body in 3-D (three-dimensional) Euclidean space
so(3): Lie algebra of SO(3), which is represented as the linear space of 3×3 skew-symmetric matrices
se(3): Semidirect product of $\mathbb{R}^3$ and so(3)
$\mathbb{R}^3$: 3-D real Euclidean vector space
$\mathbb{R}^6$: 6-D real Euclidean vector space
R: Cosine direction matrix rotating from the body-fixed frame to inertial frame
p: Position vector expressed in the inertial frame
v: Velocity expressed in the body-fixed frame
ω: Angular velocity expressed in the body-fixed frame
F_g: Gravity force expressed in the body-fixed frame
M_g: Gravitational gradient moment expressed in the body-fixed frame
μ: Earth gravitational constant
g: Pose matrix of the follower spacecraft on SE(3)
ξ: Velocity vector of the spacecraft in the body-fixed frame
Ad: Adjoint action of $g \in \mathrm{SE}(3)$ on $X \in \mathrm{se}(3)$
ad: Adjoint action of se(3)
ad$*$: Coadjoint representation of se(3)
τ_g: Known gravity vector (moments and forces) of the follower
τ_c: Control input vector (torque and force) act on the follower
h_d: Desired relative pose of the follower spacecraft to the leader
h: Relative configuration of the follower spacecraft to the leader
$\tilde{\eta}$: Logarithm mapping vector for the pose error of the follower
expm: Exponential map for matrix from se(3) to SE(3)
logm: Logarithm map for matrix from SE(3) to se(3)
$\tilde{\Theta}$: Exponential coordinate vector of the attitude tracking error of the follower spacecraft
$\tilde{\beta}$: Exponential coordinate vector of the position tracking error of the follower spacecraft
$\tilde{\xi}$: Velocity tracking error of the follower spacecraft relative to the leader
Superscript 0: States of the leader spacecraft.

Data Availability

The data used to support the findings of this study are included in this paper, and the simulation data are available from the corresponding author upon request.

Conflicts of Interest

The authors declare that there is no conflict of interest regarding the publication of this paper.

Acknowledgments

This research is funded by the Shanghai Aerospace Science and Technology Innovation Foundation (Grant No. SAST2017-020).

References

[1] J. L. Goodman, "History of space shuttle rendezvous and proximity operations," *Journal of Spacecraft and Rockets*, vol. 43, no. 5, pp. 944–959, 2006.

[2] P. Singla, K. Subbarao, and J. L. Junkins, "Adaptive output feedback control for spacecraft rendezvous and docking under measurement uncertainty," *Journal of Guidance, Control, and Dynamics*, vol. 29, no. 4, pp. 892–902, 2006.

[3] F. Zhang and G. Duan, "Robust adaptive integrated translation and rotation control of a rigid spacecraft with control saturation and actuator misalignment," *Acta Astronautica*, vol. 86, pp. 167–187, 2013.

[4] F. Zhang and G.-R. Duan, "Integrated relative position and attitude control of spacecraft in proximity operation missions," *International Journal of Automation and Computing*, vol. 9, no. 4, pp. 342–351, 2012.

[5] J. Wang and Z. Sun, "6-DOF robust adaptive terminal sliding mode control for spacecraft formation flying," *Acta Astronautica*, vol. 73, pp. 76–87, 2012.

[6] N. Filipe and P. Tsiotras, "Adaptive position and attitude-tracking controller for satellite proximity operations using dual quaternions," *Journal of Guidance, Control, and Dynamics*, vol. 38, no. 4, pp. 566–577, 2015.

[7] H. Gui and G. Vukovich, "Dual-quaternion-based adaptive motion tracking of spacecraft with reduced control effort," *Nonlinear Dynamics*, vol. 83, no. 1-2, pp. 597–614, 2016.

[8] D. Lee, A. K. Sanyal, and E. A. Butcher, "Asymptotic tracking control for spacecraft formation flying with decentralized collision avoidance," *Journal of Guidance, Control, and Dynamics*, vol. 38, no. 4, pp. 587–600, 2015.

[9] D. Lee and G. Vukovich, "Almost global finite-time stabilization of spacecraft formation flying with decentralized collision avoidance," *International Journal of Control, Automation and Systems*, vol. 15, no. 3, pp. 1167–1180, 2017.

[10] J. Zhang, D. Ye, Z. Sun, and C. Liu, "Extended state observer based robust adaptive control on se(3) for coupled spacecraft tracking maneuver with actuator saturation and misalignment," *Acta Astronautica*, vol. 143, pp. 221–233, 2018.

[11] J. Zhang, J. Biggs, and Z. Sun, "Relative orbit-attitude tracking for spacecraft using adaptive fast terminal sliding mode control," in *5th CEAS Specialist Conference on Guidance, Navigation and Control-EuroGNC*, Milano, 2019.

[12] J. Zhang, D. Ye, J. D. Biggs, and Z. Sun, "Finite-time relative orbit-attitude tracking control for multi-spacecraft with collision avoidance and changing network topologies," *Advances in Space Research*, vol. 63, no. 3, pp. 1161–1175, 2019.

[13] L. Sun and W. Huo, "Robust adaptive relative position tracking and attitude synchronization for spacecraft rendezvous," *Aerospace Science and Technology*, vol. 41, pp. 28–35, 2015.

[14] L. Sun and W. Huo, "6-DOF integrated adaptive backstepping control for spacecraft proximity operations," *IEEE Transactions on Aerospace and Electronic Systems*, vol. 51, no. 3, pp. 2433–2443, 2015.

[15] L. Sun, W. Huo, and Z. Jiao, "Disturbance-observer-based robust relative pose control for spacecraft rendezvous and proximity operations under input saturation," *IEEE Transactions on Aerospace and Electronic Systems*, vol. 54, no. 4, pp. 1605–1617, 2018.

[16] Y. Huang and Y. Jia, "Adaptive fixed-time relative position tracking and attitude synchronization control for non-cooperative target spacecraft fly-around mission," *Journal of the Franklin Institute*, vol. 354, no. 18, pp. 8461–8489, 2017.

[17] Y. Huang and Y. Jia, "Adaptive fixed-time six-DOF tracking control for noncooperative spacecraft fly-around mission," *IEEE Transactions on Control Systems Technology*, vol. 27, no. 4, pp. 1796–1804, 2019.

[18] Y. Huang and Y. Jia, "Robust adaptive fixed-time tracking control of 6-DOF spacecraft fly-around mission for noncooperative target," *International Journal of Robust and Nonlinear Control*, vol. 28, no. 6, pp. 2598–2618, 2018.

[19] A. Sanyal, N. Nordkvist, and M. Chyba, "An almost global tracking control scheme for maneuverable autonomous vehicles and its discretization," *IEEE Transactions on Automatic Control*, vol. 56, no. 2, pp. 457–462, 2011.

[20] J. E. Marsden and T. S. Ratiu, *Introduction to Mechanics and Symmetry*, Springer, New York, 1999.

[21] J. D. Biggs and L. Colley, "Geometric attitude motion planning for spacecraft with pointing and actuator constraints," *Journal of Guidance, Control, and Dynamics*, vol. 39, no. 7, pp. 1672–1677, 2016.

[22] D. Lee, A. Sanyal, E. Butcher, and D. Scheeres, "Finite-time control for spacecraft body-fixed hovering over an asteroid," *IEEE Transactions on Aerospace and Electronic Systems*, vol. 51, no. 1, pp. 506–520, 2015.

[23] A. Sanyal, L. Holguin, and S. P. Viswanathan, "Guidance and control for spacecraft autonomous chasing and close proximity maneuvers," *IFAC Proceedings Volumes*, vol. 45, no. 13, pp. 753–758, 2012.

[24] M. Nazari, E. A. Butcher, T. Yucelen, and A. K. Sanyal, "Decentralized consensus control of a rigid-body spacecraft formation with communication delay," *Journal of Guidance, Control, and Dynamics*, vol. 39, no. 4, pp. 838–851, 2016.

[25] L. Holguin, S. P. Viswanathan, and A. Sanyal, "Guidance and control for spacecraft autonomous rendezvous and proximity maneuvers using a geometric mechanics framework," in *AIAA Guidance, Navigation, and Control Conference American Institute of Aeronautics and Astronautics*, Minneapolis, Minnesota, August 2012 - 16 August 2012.

[26] L. Jiang, Y. Wang, and S. Xu, "Integrated 6-dof orbit-attitude dynamical modeling and control using geometric mechanics," *International Journal of Aerospace Engineering*, vol. 2017, Article ID 4034328, 13 pages, 2017.

[27] B. Jiang, Q. Hu, and M. I. Friswell, "Fixed-time attitude control for rigid spacecraft with actuator saturation and faults," *IEEE Transactions on Control Systems Technology*, vol. 24, no. 5, pp. 1892–1898, 2016.

[28] B. Huang, A.-j. Li, Y. Guo, and C.-q. Wang, "Fixed-time attitude tracking control for spacecraft without unwinding," *Acta Astronautica*, vol. 151, pp. 818–827, 2018.

[29] J. Gao and Y. Cai, "Fixed-time control for spacecraft attitude tracking based on quaternion," *Acta Astronautica*, vol. 115, pp. 303–313, 2015.

[30] Q. Hu, W. Chen, and L. Guo, "Fixed-time maneuver control of spacecraft autonomous rendezvous with a free-tumbling target," *IEEE Transactions on Aerospace and Electronic Systems*, vol. 55, no. 2, pp. 562–577, 2019.

[31] D. Lee, G. Vukovich, and H. Gui, "Adaptive variable-structure finite-time mode control for spacecraft proximity operations with actuator saturation," *Advances in Space Research*, vol. 59, no. 10, pp. 2473–2487, 2017.

[32] J. Wu, K. Liu, and D. Han, "Adaptive sliding mode control for six-DOF relative motion of spacecraft with input constraint," *Acta Astronautica*, vol. 87, pp. 64–76, 2013.

[33] Y. Lv, Q. Hu, G. Ma, and J. Zhou, "6 DOF synchronized control for spacecraft formation flying with input constraint and

parameter uncertainties," *ISA Transactions*, vol. 50, no. 4, pp. 573–580, 2011.

[34] Q. Hu, G. Ma, and L. Xie, "Robust and adaptive variable structure output feedback control of uncertain systems with input nonlinearity," *Automatica*, vol. 44, no. 2, pp. 552–559, 2008.

[35] Q. Hu, "Robust adaptive sliding mode attitude maneuvering and vibration damping of three-axis-stabilized flexible spacecraft with actuator saturation limits," *Nonlinear Dynamics*, vol. 55, no. 4, pp. 301–321, 2009.

[36] J. D. Boĭskovic, S.-M. Li, and R. K. Mehra, "Robust adaptive variable structure control of spacecraft under control input saturation," *Journal of Guidance, Control, and Dynamics*, vol. 24, no. 1, pp. 14–22, 2001.

[37] J. L. Junkins and H. Schaub, *Analytical Mechanics of Space Systems*, American Institute of Aeronautics and Astronautics, Second Edition edition, 2009.

[38] F. Bullo and R. M. Murray, "Proportional derivative (pd) control on the Euclidean group," in *European Control Conference Citeseer*, pp. 1091–1097, Zurich, Switzerland, September 1995.

[39] A.-M. Zou, K. D. Kumar, Z.-G. Hou, and X. Liu, "Finite-time attitude tracking control for spacecraft using terminal sliding mode and Chebyshev neural network," *IEEE Transactions on Systems, Man, and Cybernetics, Part B (Cybernetics)*, vol. 41, no. 4, pp. 950–963, 2011.

[40] Z. Zuo, "Non-singular fixed-time terminal sliding mode control of non-linear systems," *IET Control Theory & Applications*, vol. 9, no. 4, pp. 545–552, 2015.

[41] J. Ni, L. Liu, C. Liu, X. Hu, and S. Li, "Fast fixed-time nonsingular terminal sliding mode control and its application to chaos suppression in power system," *IEEE Transactions on Circuits and Systems II: Express Briefs*, vol. 64, no. 2, pp. 151–155, 2017.

[42] D. Lee and G. Vukovich, "Robust adaptive terminal sliding mode control on SE(3) for autonomous spacecraft rendezvous and docking," *Nonlinear Dynamics*, vol. 83, no. 4, pp. 2263–2279, 2016.